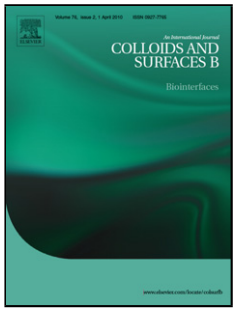

Title: Synthetic anionic surfaces can replace microparticles in stimulating burst coagulation of blood plasma

Authors: Angel Contreras-García, Noelia D'Elia, Maxime Desgagné, Charles-Hubert Lafantaisie-Favreau, Georges-Etienne Rivard, Juan-Carlos Ruiz, Michael R. Wertheimer, Paula Messina, Caroline D. Hoemann

PII: S0927-7765(18)30848-8
DOI: https://doi.org/10.1016/j.colsurfb.2018.11.066
Reference: COLSUB 9831

To appear in: *Colloids and Surfaces B: Biointerfaces*

Received date: 18 June 2018
Revised date: 23 October 2018
Accepted date: 26 November 2018

Please cite this article as: { https://doi.org/

Synthetic anionic surfaces can replace microparticles in stimulating burst coagulation of blood plasma

Angel Contreras-García[1], Noelia D'Elia[2,3], Maxime Desgagné[2], Charles-Hubert Lafantaisie-Favreau[2], Georges-Etienne Rivard[4], Juan-Carlos Ruiz[5], Michael R. Wertheimer[1,6], Paula Messina[3], Caroline D. Hoemann[2,6,7]*

[1]Groupe de Physique et Technologie des Couches Minces (GCM), Department of Engineering Physics, École Polytechnique de Montréal, Montreal, QC, Canada, H3C 3A7

[2]Department of Chemical Engineering, École Polytechnique de Montréal, Montreal, QC, Canada H3C 3A7

[3]Department of Chemistry, Universidad Nacional del Sur, CONICET, 8000 Bahia Blanca, Argentina.

[4]Hematology Oncology, CHU Sainte-Justine, Montreal, QC, Canada H3T 1C5

[5]División de Ciencias Básicas e Ingeniería, Depto. de Ingeniería de Procesos e Hidráulica, Universidad Autónoma Metropolitana-Iztapalapa, Av. San Rafael Atlixco No. 186, 09340 México D.F., Mexico

[6]Institute of Biomedical Engineering, École Polytechnique de Montréal, C.P. 6079, Succursale Centre-Ville, Montréal, QC H3C 3A7, Canada

[7]Department of Bioengineering, George Mason University, Manassas, VA, USA.

*Corresponding author and current address:

Caroline D. Hoemann, Ph.D.
Department of Bioengineering
Volgenau School of Engineering
Institute of Advanced Biomedical Research
10900 George Mason Circle
George Mason University
Manassas, VA, USA 20110
E-mail: choemann@gmu.edu

Graphical abstract

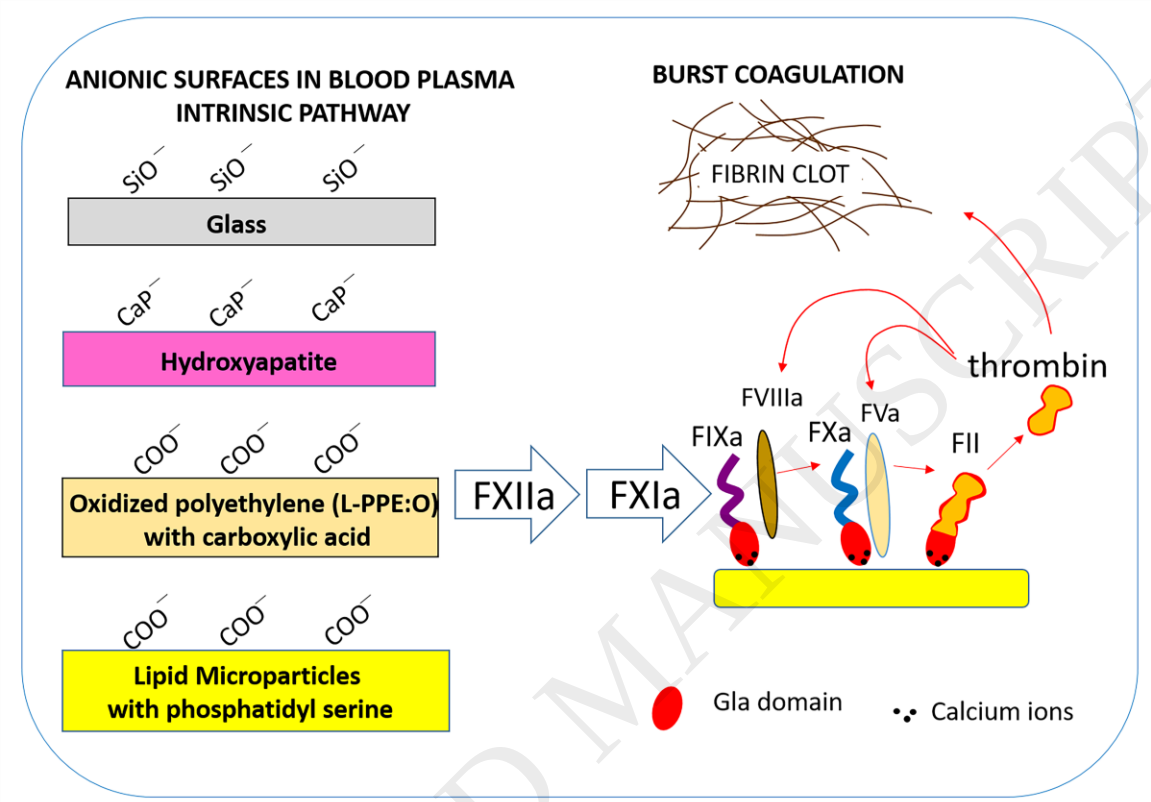

Highlights

- Microparticle-depleted blood plasma failed to coagulate in plastic cups
- Polyethylene-carboxylate L-PPE:O nanocoatings were created by glow-discharge plasma
- Hydroxyapatite particles, glass microbeads, and L-PPE:O coatings had anionic surfaces
- Anionic surfaces induced burst coagulation of microparticle-depleted plasma via FXII
- Microparticles and anionic surfaces can activate thrombin without platelet activation

Abstract

Biomaterials are frequently evaluated for pro-coagulant activity but usually in the presence of microparticles (MPs), cell-derived vesicles in blood plasma whose phospholipid surfaces allow coagulation factors to set up as functional assemblies. We tested the hypothesis that synthetic anionic surfaces can catalyze burst thrombin activation in human blood plasma in the absence of MPs. In a thromboelastography (TEG) assay with plastic sample cups and pins, recalcified human citrated platelet-poor plasma spontaneously burst-coagulated but with an unpredictable clotting time whereas plasma depleted of MPs by ultracentrifugation failed to coagulate. Coagulation of MP-depleted plasma was restored in a dose-dependent manner by glass microbeads, hydroxyapatite nanoparticles (HA NPs), and carboxylic acid-containing anionic nanocoatings of TEG cups and pins (coated by glow-discharge plasma-polymerized ethylene containing oxygen, L-PPE:O with 4.4 and 6.8 atomic % [COOH]). Glass beads lost their pro-coagulant activity in MP-depleted plasma after their surfaces were nanocoated with plasma-polymerized hexamethyl disiloxane (PP-HMDSO). In FXII-depleted MP-depleted plasma, glass microbeads failed to induce coagulation, however, FXIa was sufficient to induce coagulation in a dose-dependent manner, with no effect of glass beads. These data suggest that anionic surfaces of crystalline, organic, and amorphous solid synthetic materials catalyze explosive thrombin generation in MP-depleted plasma by activating the FXII-dependent intrinsic contact pathway. The data also show that microparticles are pro-coagulant surfaces whose activity has been largely overlooked in many coagulation studies to-date. These results suggest a possible mechanism by which anionic biomaterial surfaces induce bone healing by contact osteogenesis, through fibrin clot formation in the absence of platelet activation.

Keywords: blood coagulation; hydroxyapatite; microparticles; thromboelastography; plasma enhanced chemical vapor deposition (PECVD); thrombin; FXII; FXIa; contact pathway, contact osteogenesis

1. Introduction

Biomaterial-induced blood coagulation can lead to either therapeutic or adverse effects, therefore, the mechanisms governing biomaterial-induced coagulation should be thoroughly understood. Thromboelastography (TEG) is an *in vitro* assay used to study the effect of biomaterials on blood coagulation, and typically uses unmodified whole blood, citrated whole blood, or citrated blood plasma [1-5]. In the TEG assay, a liquid blood sample is deposited in a heated plastic cup and a plastic pin attached to a torsion wire is immersed in the sample. The cup oscillates at a fixed angle and when fibrin strands start to connect the cup and the pin, the torsion wire begins to rotate with the cup giving rise to a symmetric trace with an amplitude that is proportional to the viscoelastic clot tensile strength [6] (Fig 1). Thrombin activation dynamically parallels the TEG trace amplitude (parameter A) [7], meaning that explosive thrombin generation can be indirectly demonstrated by a sigmoidal curve which is usually accompanied by a sharp angle ($\alpha \geq 30°$) in the TEG trace (Fig. 1). Biomaterials and clotting factors introduced in the TEG assay can alter clotting time, α, and TEG trace amplitude, with corresponding alterations in thrombin activation kinetics [2].

Citrated platelet-poor plasma (PPP), like citrated whole blood, can be recalcified *in vitro* and will spontaneously burst coagulate in the TEG assay but with a variable clot initiation time [5]. PPP coagulates faster with more precise kinetics when the conventional plastic Cyrolite® TEG cup and pin are coated with anionic carboxylic acid (COOH)-rich nanolayers termed L-PPE:O (low-pressure plasma polymerized ethylene containing oxygen); these nanolayers consist of oxidized polyethylene and are generated by glow-discharge plasma-enhanced chemical vapor deposition (PECVD) [5]. It is important to distinguish between *blood plasma* and gaseous *glow-discharge plasma* and in this text; hereafter, we shall mostly be referring to the former. Other PECVD nanolayers, including hydrophilic amine-containing (L-PPE:N), "glass-like" (PP-SiO_2)

and hydrophobic (PP-HMDSO), failed to accelerate PPP coagulation [5]. The mechanisms behind the pro-coagulant effect of L-PPE:O remain unclear. The purpose of this study was therefore to elucidate the mechanisms of anionic surface-induced PPP coagulation in the TEG assay. Our long-term goal is to develop a novel functional bioassay for testing the potential for different biomaterials to influence burst thrombin activation in citrated plasma samples, using pooled qualified blood plasma as a standard, and plasma from distinct individuals for precision medicine.

Citrated plasma is cleared of blood cells and most platelets by low-speed centrifugation but it still contains microparticles (MPs) and trace platelets (reviewed in [8, 9]). MPs (also called "platelet dust", exosomes, extracellular vesicles) are phospholipid vesicles that are shed into the blood circulation from a variety of cell types including platelets, erythrocytes, leukocytes, and endothelial cells [10]. Ultracentrifugation can be used to collect MPs, and MPs from normal citrated plasma have modest pro-coagulant activity while MPs collected from individuals with pro-inflammatory states (sepsis, cardiac by-pass, kidney disease, heparin-induced thrombocytopenia) have relatively higher pro-coagulant activity [11-16]. As MPs are derived from multiple cell sources, it is important to note that MPs arising from different cell sources initiate and propagate coagulation through different mechanisms. Platelet-derived MPs (CD61+) display variable phosphatidyl serine (PS) content on their outer surface [13, 17]. PS is normally located on the inner cell membrane and upon platelet activation a flippase/scramblase transfers PS to the external membrane leaflet. PS carries a unique anionic carboxylic acid charge group that serves as an essential docking site that tethers and orients the calcium-binding γ-carboxyglutamic acid (gla) domain of key coagulation factors (FVII, FIX, FX, FII/prothrombin, Protein C), so that their active sites and sessile bonds are at an optimal distance from the plasma membrane (*i.e.,* 52 to 90 Å) [18, 19]. Granulocyte- (CD66b+) and monocyte-derived (CD14+) MPs express different levels of Tissue Factor (TF) [8, 13]. TF is a transmembrane co-factor that complexes with FVIIa, a gla

domain serine protease that when complexed with TF directly activates FIX and FX to create tenase and prothrombinase, respectively [20, 21]. To summarize, MPs in normal blood plasma have features that facilitate coagulation by contributing trace PS+ binding sites for cooperative assembly of tenase, prothrombinase, and prothrombin, and potentially trace TF [8, 13].

In order to test the hypothesis that MPs are required to initiate burst coagulate of PPP in the TEG assay, we used ultracentrifugation (136,000xg) to produce MP-depleted and MP-enriched plasma. Samples were recalcified and allowed to coagulate in the TEG assay using commercially supplied Cyrolite® plastic cups and pins. Our first experiments showed that PPP and PPP enriched 2-fold for MPs spontaneously burst-coagulated, while MP-depleted plasma failed to coagulate in the plastic TEG cups. We then tested the hypothesis that synthetic anionic surfaces stimulate coagulation of PPP, and are necessary and sufficient to induce coagulation of MP-depleted plasma. Our results showed that MP-depleted plasma burst coagulated solely in contact with anionic surfaces, and that the effect was sensitive to the anion charge density. We also provide evidence using FXII-depleted plasma spiked with FXIa that anionic surfaces induce burst coagulation of MP-depleted plasma by activating the contact (FXII-dependent) pathway.

2. Methods

2.1 Materials

Plastic TEG cups and pins made of Cyrolite®, a methacrylate-based polymer, were purchased from Haemonetics Corporation (IN, USA) or Hemoscope (IN, USA). Other reagents included 10 µm-diameter carboxylated CML latex beads at 4% w/v (Life Technologies, Cedarlane, ON, Canada, Product No. C37259, Lot No. 1071765 with $6.8x10^8$ COOH groups per particle), 10 µm diameter dark red latex beads at 2% w/v (Sigma-Aldrich, Oakville, ON, Canada, Product No. 61946), 10 µm diameter borosilicate glass beads (SPHERICEL® Hollow 10 µm Glass Spheres, Grade 110P8, Matweb), synthetic HA nanoparticle rods of 40 nm x 9 nm created with CTAB and IGEPAL (2.03 Ca/P ratio) [22], and $CaCl_2$ (Sigma-Aldrich, Oakville, ON, Canada, Product No. C5670 dihydrate or C7902 anhydrous) to prepare 200 mM $CaCl_2$ (osmolality of 490 to 510 mOsm). The 4% w/v latex bead, CML bead, and glass microbead suspensions were generated at 2.5 mg/mL in 200 mM $CaCl_2$ to obtain an average 4.25±0.75 million beads per mL 200 mM $CaCl_2$ as verified with a Countess Automated cell counter (Invitrogen, Thermo-Fisher, Canada). HA nanoparticles were suspended in ddH_20 at 0.25, 2.5, and 25 mg/mL and characterized for zeta potential in 0.01 M NaCl solution pH 7.0 in triplicate.

2.2. PECVD thin film coatings of TEG cups and pins and glass beads

The inner surface of the TEG cups and outer surface of the TEG pins were coated using PECVD to make ~200 nm thick nanocoatings with hydrophobic character (PP-HMDSO, plasma-polymerized hexamethyldisiloxane), or hydrophilic anionic character (L-PPE:O), at distinct oxygen/ethylene gas flow ratios, $R \equiv O_2/C_2H_4$ of 0.025, 0.05, and 0.075) as previously described [5]. Briefly, TEG cups and pins were placed in custom aluminum holders on the lower plate electrode of an aluminum/steel vacuum chamber, and under low pressure ($<10^6$ Torr), the chamber

was filled with a flowing gas mixture of ethylene (99.5%) and 10% oxygen/90% argon gas mixture (for L-PPE:O), or pure HMDSO (99.7%) vapor for (PP-HMDSO) while controlling the applied 13.56 MHz radio-frequency power (ca. 10 Watts) and operating pressure (ca 600 mTorr) to create the ~200 nm thick coatings. Small pieces of single-crystal silicon (c-Si) wafer were placed on the aluminum holders during deposition runs as test surfaces for water contact angle measurements. Glass beads (500 µm diameter, Zymogen, QC, Canada) were also coated as a single bead layer with PP-HMDSO using the same parameters, then part-way through the coating, the glass beads were moved one by one and the PECVD treatment repeated so that all bead surfaces were coated.

2.3. Characterization of coatings

X-ray photoelectron spectroscopy (XPS)

The TEG cups and L-PPE:O-modified TEG cup surfaces were characterized by high resolution X-ray Photoelectron Spectroscopy (HR XPS) (VG ESCALAB 3MkII instrument, using non-monochromatic Mg Kα radiation) directly on the bottom of the TEG cup [5]. Functional concentrations were determined using Avantage v4.12 software (Thermo Electron Corp.) by integration of the area under specific sub-peaks following subtraction of a Shirley-type background. O1s was fitted with two peaks (O=C (532.4 eV) and O-C (533.9 eV) while C1s was fitted with 5 peaks, A, B, C (285.0, C-C, C=C; 285.7, C-COOR; 286.6 eV, C-OR; respectively), peak D (C=O, 287.9 eV) and E (COOR, 289.2 eV). The oxygen content of Cyrolite® and PP-HMDSO thin films was previously reported [5]. The carboxylic acid/ester content of the L-PPE:O surfaces was quantified by calculating the area under the HR-XPS C1s peak at 289.2 eV (Avantage v4.12 software). COOR content of CML beads was determined using the same approach. Calcium content of borosilicate glass beads, and surface character of 500 µm glass bead surfaces before and after PP-HMDSO coating were also analyzed by XPS.

Contact angle goniometry (CAG)

CAG measurements determine the angle between a surface and the tangent made with it by a small water droplet deposited on the surface. CAG using water gives a rough indicator of surface wettability. Note that hydrophilicity is not a precise notion, because CA depends not only on chemistry, but also on surface morphology (roughness). Generally, if the WCA is >90°, the solid surface is considered hydrophobic. CAG measurements were carried out with a dedicated goniometer (Ramé-Hart, Inc.) on a flat part of the TEG cup (Cyrolite®), or on a PECVD deposit made on a piece of c-Si wafer, and reproducibility was verified by repeating the procedure 3 times.

2.4 Thromboelastography assays.

Assays were carried out in three tandem TEG 5000 thromboelastograph instruments (Haemonetics Corporation, Niles, IL, USA), permitting the simultaneous analysis of six samples, or a single TEG 5000 analyzer (FXII-depleted plasma assays). Citrated PPP containing 3.2% w/v citrate (CRYOcheck®, Catalog number: CNN-15, lot# A1104, Precision BioLogic, Dartmouth, Nova Scotia, Canada, confirmatory experiments with lot# A1151) collected by apheresis from consented healthy human donors and pooled, was characterized as containing 2.90 or 3.34 g/L fibrinogen, and from 92% to 118% FII, FV, FVII, VIII, FIX, FX, FXI, and FXII (according to the Certificates of Analysis), and platelet counts less than 1 million per mL (personal communication Stephen Yorke, Technical Support, Precision BioLogic). Plasma was received frozen on dry ice in 1.5 mL aliquots, was stored at -80ºC, and thawed at 37ºC for 5 minutes prior to use. TEG instruments were verified by e-tests prior to each experiment. MP-depleted plasma was generated as follows: 1 mL PPP was ultra-centrifuged for 30 minutes at 50,000 rpm (136,000xg) at 4°C in a fixed angle rotor TLA-110 (Optima Max-E Beckman Ultracentrifuge) in 1.5 mL Microfuge® polyallomer tubes (Beckman Product No. 357448), and 0.5 mL supernatant (MP-depleted plasma) was carefully

recovered avoiding any floating lipids, while MP-enriched plasma consisted of the resulting pellet containing MPs resuspended by vortexing in the remaining 0.5 mL PPP. TEG assays in unmodified and PECVD-modified TEG cups were run by depositing 20 μL of 200 mM $CaCl_2$ in the TEG cup, followed by 340 μL of citrated platelet-poor plasma (PPP), MP-enriched, or MP-depleted plasma. Other assays were performed with 20 μL of 200 mM $CaCl_2$ containing 2.5 mg/mL microbeads and 340 μL plasma, or 20 μL of 200 mM $CaCl_2$, 20 μL of ddH_20 with or without HA NPs (0.25, 2.5 or 25 mg/mL) and 320 μL plasma. The volume of plasma in the TEG cups was kept constant regardless of the number and volume of substances added, either 320 μL (HA NPs) or 340 μL (all other conditions) (Table 1). Microbead and HA NP suspensions were vortexed immediately prior to pipetting into the TEG cup. TEG assays were also carried out using citrated FXII-depleted plasma (catalog number FDP12-10, Lot D12-34, pooled PPP immunoadsorbed to deplete FXII to <1%, HEPES buffered, frozen; Precision BioLogic). Plasma was thawed at 37°C, depleted of MPs by ultracentrifuging at 50,000xrpm as described above, then the coagulation assay performed by pipetting into the TEG cup: 20 μL of 200 mM $CaCl_2$ ± 2.5 mg/mL glass microbeads, 20 μL of ddH_20, or 20 μL FXIa (Haematologic Technologies, VT, USA; diluted 1:500, 1:5000 or 1:12,500 in ddH_20 from a 591 U/mg, 5.1 mg/mL stock), then 320 μL FXII-depleted MP-depleted plasma.

2.5 Environmental Scanning Electron Microscopy (ESEM)

MPs were pelleted by ultra-centrifugation (136,000xg, 30 minutes, 4°C), then re-suspended in 100 μL supernatant by 20 seconds of vortex mixing, fixed by adding excess 2% glutaraldehyde/0.1 M sodium cacodylate pH 7.3, washed twice in ddH_20 (ultra-centrifuging each time), then transferred to an ESEM stage and imaged under high vacuum in a Quanta 200 field-emission gun (FEG) environmental scanning electron microscope (ESEM). PPP and MP-depleted plasma clots were formed in the presence of glass microbeads for 70 minutes at 37°C with light agitation, fixed in

2% glutaraldehyde/0.1 M sodium cacodylate pH 7.3, washed 3 times 5 min. in ddH_20, dehydrated in graded ethanol series followed by amyl acetate/ethanol, submitted the Facility for Electron Microscopy Research (McGill University, Montreal, Canada) for critical-point drying, then submitted to the following gold sputtering parameters: 80 seconds (<8 nm thickness), pump pressure 0.08 mBar, sputter current: 30 mAmp, table position: at 30 mm target to sample distance, and analyzed under high vacuum mode at 10 kV by ESEM.

2.6 Statistical Analyses

Data are presented as mean (marker) ± standard error (bars) ± standard deviation of the mean (whiskers). Differences in TEG parameters R, α (alpha) and MA were evaluated using the General Linear Model with an Unequal N Honest Significant Differences (HSD) post-hoc test (Statistica v12, Tulsa, OK, USA). Sample numbers for PPP samples were as follows: Cyrolite TEG cup N=14, HMDSO-coated TEG cups N=6, latex beads N=3, carboxylated CML latex beads N=6, glass beads N=8, HA at 25 mg/mL N=5, L-PPE:O coated TEG cups at R=0.075 N=5, MP-enriched plasma N=10. Sample numbers for MP-depleted plasma were as follows: Cyrolite TEG cup N=11, HMDSO coating N=4, latex beads, N=4, carboxylated CML latex beads N=6, glass microbeads N=7, HA NPs N=4, L-PPE:O coating (R=0.075) N=8. MP-enriched PPP N=9. The level of significance was set at p = 0.05.

3. Results

MPs pelleted from citrated PPP by ultracentrifugation and fixed in glutaraldehyde formed circular sub-micron aggregated structures (Fig. 2A). In the TEG assay with standard plastic cups and pins, PPP and PPP 2-fold enriched for MPs (E-PPP) spontaneously coagulated with burst

kinetics proportional to MP concentration, whereas MP-depleted plasma failed to coagulate (Fig. 2B).

TEG cups and pins were modified by PECVD to have surfaces with different levels of [COOH] by step-wise increases in the O_2/C_2H_2 gas flow ratio (*R*=0.025, 0.05, and 0.075*)*; the resulting L-PPE:O surfaces had increasing wettability as shown by a progressive decrease in water contact angle (WCA 64°, 51° and 45°, respectively, Table 2), along with a progressive increase in oxygen content, [O] ([O] = 14.3, 24.4, and 29.8 atomic % (at%)). L-PPE:O *R*=0.05 had [O] comparable to that of Cyrolite ([O] = 22.3 at%, Table 3). It is important to note that one L-PPE:O surface with the lowest oxygen level had zero [COOH] content, while the other two L-PPE:O surfaces had 4.4, and 6.8 at% [COOH}, respectively (peak E, Table 4, Fig. 3). Uncoated Cyrolite was more hydrophobic (WCA 77°) and HMDSO-coated surfaces were hydrophobic (WCA 98°, Table 2), which is consistent with a lack of free hydroxyl (OH) or carboxylic acid (COOH) groups in the methacrylate-based Cyrolite or in PP-HMDSO organosilicone film coatings (Table 4) [5].

The anionic character of L-PPE:O thin layers with 6.8 at% [COOH] immersed in water has been previously established (-15 V surface potential) [5]. Another experimental anionic material consisted of HA NPs with a Ca/P ratio of 2.03 [22]. HA NPs showed a zeta potential of -6.19 ± 0.83 mV in 10 mM NaCl of pH=7.0. Borosilicate glass (SiO^-) has an anionic surface in aqueous solution [23] that promotes the FXII-dependent contact pathway [24]. As calcium is essential for coagulation, it is interesting to note that the HA NPs showed a structure of $Ca_{10}(PO_4)_6(OH)_2$ [22], and according to XPS analyses, glass microbeads showed a calcium content of 2.4 at% Ca2p3 (peak signal at 248.3 eV).

PPP showed an average 16 ±6 minute clot initiation time in standard plastic Cyrolite TEG cups and pins, whereas HA NPs accelerated PPP coagulation in a dose-dependent manner, with

optimal stimulation at 2 mg/mL (parameter R, Fig. 4A). At the optimal concentration, all three anionic surfaces (2 mg/mL HA NPs, 0.2 mg/mL glass beads, L-PPE:O with 6.8 at% [COO^-] shortened PPP coagulation time to precisely 9±1 minutes ($p<0.05$ to 0.01 *vs* all other surfaces, Fig. 4B). Hydrophobic surfaces (HMDSO coatings, latex beads), and mixed hydrophobic/hydrophilic surfaces (CML beads), delayed the average PPP clot initiation time to between 19 and 23 minutes (black boxes, Fig. 4B). PPP burst-coagulated with an average alpha 38°±16° that was depressed by hydrophobic surfaces to between 23° and 29°, and amplified by anionic surfaces to have consistently high α values of 62°±4° (glass beads), 60°±4° (HA NPs), and 53°±6° (L-PPE:O) ($p<0.05$ to 0.001 *vs* all other surfaces, open boxes, Fig. 4B). The maximal amplitude (MA) value, which reflects clot tensile strength was not significantly altered by any of the surfaces (grey boxes, Fig. 4). To summarize, these data showed that all three anionic surfaces promoted a faster and more reproducible burst coagulation of PPP which contains MPs and trace platelets *(i.e.,* less than 1 million platelets per mL *versus* 143 to 450 million platelets per mL in normal human whole blood [25]).

Remarkably, synthetic anionic surfaces restored burst coagulation of MP-depleted plasma in a dose-dependent manner. L-PPE:O nano-coatings initiated coagulation according to carboxylic acid content, with an average clotting time of 18 minutes and $\alpha = 32°$ for 4.4 at% [COO^-], and a more rapid clotting time of 11 minutes and $\alpha = 48°$ for 6.8 at% [COO^-] (Fig. 5A). Most importantly, L-PPE:O surfaces devoid of [COO^-] failed to induce coagulation of MP-depleted plasma (R=0.025, Fig. 5A). HA NPs induced burst coagulation of MP-depleted plasma at 2 mg/mL (but not lower concentrations), with a relatively slower clotting time of 24 minutes and $\alpha = 37°$ (Fig. 5). Glass microbeads induced burst coagulation of MP-depleted plasma at 0.2 mg/mL, with a clotting time of 17 minutes and $\alpha = 40°$ (Fig. 5B). Glass beads coated with HMDSO by PECVD

no longer induced coagulation of MP-depleted plasma, ruling out surface curvature as a factor (data not shown; Table 5). Among all anionic surfaces, L-PPE:O coatings with 6.8 at% [COO^-] induced the shortest clotting time (11 minutes), and highest α (48°) of MP-depleted plasma (Fig. 6A). Clot tensile strength was similar for PPP, E-PPP, and MP-depleted plasma induced to coagulate with anionic surfaces (Fig. 5B). To summarize, these data showed that organic (L-PPE:O), crystalline (HA NPs), and amorphous solid (glass microbead) synthetic anionic surfaces had a similar *in vitro* pro-coagulant activity as MPs.

Given that anionic surfaces activate FXII and induce the contact pathway, we evaluated the potential role of the contact pathway in coagulation of MP-depleted plasma. We used used FXIa, the factor immediately downstream of FXIIa, to by-pass FXII and initiate coagulation in FXII-depleted, MP-depleted plasma. As expected, calcium or calcium with glass beads failed to induce coagulation (Fig. 6B). FXIa stimulated a dose-dependent burst coagulation of FXII-depleted plasma, MP-depleted plasma, with no effect of glass beads (Fig. 6B). These data showed that activation of the contact pathway is sufficient to induce burst coagulation of MP-depleted plasma.

Fibrin clot fiber structure was examined at high-magnification in PPP and MP-depleted plasma coagulated in the presence of glass microbeads. A meshwork of fibrin fibers enveloped the glass beads (Fig. 7A & D). Thick and thin fibrin fibers adhered to the glass beads in both PPP clots and MP-depleted plasma clots (Fig. 7A-B vs 7D-E). Fibrin networks formed in PPP and MP-depleted plasma in the presence of glass beads had a similar structure (Fig. 7C vs 7F), except for the presence of sub-micron spherical aggregates near the surface of the PPP clot that could represent lipid micelle aggregates (Fig. 7C).

4. Discussion

This study has generated new knowledge of the inherent potential for synthetic anionic surfaces to initiate and propagate burst coagulation of citrated plasma. Our data reveal a previously unsuspected ability of calcium phosphate minerals, glass beads, and carboxylated surfaces to substitute for anionic phospholipid surfaces normally provided by MPs in platelet-poor plasma [16]. Seminal experiments by Ratnoff showed that anionic glass surfaces activate the contact pathway in blood plasma through FXII [28]. More recently, it was suggested that hydrophobic surfaces also have the potential to activate the contact pathway through factor XII activation [24], however these previous studies were carried out using PPP [29] which also contains MPs. In the present study, we showed that MPs were necessary and sufficient to induce burst coagulation of recalcified citrated plasma. These results are consistent with the findings of Wang et al [27] showing that murine neutrophil-shed MPs stimulate thrombin generation through a FXII-dependent pathway. We furthermore showed that hydrophobic surfaces and polar uncharged surfaces (Latex beads, CML beads, L-PPE:O R=0.025 with 0 at.% [COO^-]) failed to accelerate coagulation of PPP, and also failed to induce coagulation of MP-depleted plasma. Anionic surfaces could substitute for MPs in initiating coagulation of MP-depleted plasma, provided that the contact pathway was initiated (i.e., FXIa). The resulting fibrin clot structure was similar for PPP and MP-depleted plasma fibrin clots. From the collective data, we conclude that synthetic anionic surfaces analyzed in this study induced burst coagulation of MP-depleted plasma with kinetics related to their rates of FXIIa and FXIa generation.

Data generated in this study and others suggest that MP surfaces present in normal pooled human citrated blood plasma have a similar ability to stimulate the contact pathway as a variety of synthetic anionic surfaces, including glass, L-PPE:O and HA NPs. These overall findings are

important because many historical coagulation experiments have over-looked MPs as contributors to contact-activation in samples that are often citrated PPP. These data add new information to growing evidence that MPs participate in mediating large thrombus formation, by generating FXII at a distance from cell surfaces . The effect could be more relevant in context of stagnant blood flow such as a compressed wound, because otherwise the MPs would be carried away by the circulation from the bleeding site.

Numerous studies have shown that FXII, the first enzyme of the contact pathway, is activated by anions such as poly-phosphates liberated from platelets, by glass, ellagic acid, kaolin, carboxylated anionic polystyrene nanoparticles, long-chain non-saturated fatty acids (stearate), dextran sulfate, as well as more recently MPs with surface-exposed PS [1, 16, 24, 27, 28, 31-35]. During the initiation phase of the contact pathway, anionic surfaces adsorb FXII, as well as high molecular weight kininogen (HMWK), a cofactor that circulates as HMWK-prekallikrein (PK) and HMWK-FXI dimer complexes [34, 36, 37]. It is believed that surface-adsorbed FXII undergoes allosteric changes that expose the active site of the zymogen without proteolytic cleavage, which permits FXII to activate PK to kallikrein [26]. This model is supported by the observation that in FXII-deficient plasma, anionic surfaces cannot convert PK to kallikrein [38]. FXII adsorbed to anionic surfaces renders FXII 50-times more susceptible to proteolytic activation, notably by kallikrein in the presence of HMWK . This sets up a reciprocal FXIIa and kallikrein activation on the anionic surface as well as FXIIa activation of FXI/HMWK to FXIa/HMWK [38]. All of these steps can occur in the absence of calcium [37]. When contact activation takes place in the presence of calcium, the common pathway is directly launched: FXIa converts FIX to FIXa (tenase) by 2 cleavages [41], then FIX converts FX to FXa (prothrombinase), and then prothrombinase cleaves FII (prothrombin) to form thrombin.

The common pathway reactions are spatially coordinated due to conserved gla domains in FIX, FX and FII that allow the factors to become concentrated on PS+ membranes. In previous studies, platelet-derived poly-phosphate, anionic carboxylated nanobeads, and kaolin accelerated coagulation of PPP in a dose-dependent manner at 0.02 to 0.5 mg/mL [31, 32, 42], similar concentrations as the glass microbeads and HA NPs analyzed in this study. It is noteworthy that all three of these surfaces stimulated PPP coagulation with a kinetics very similar to that reported by Fletcher et al. for kaolin-activated human pooled PPP (R=9.4 minutes, α=52°, MA=24.6 mm) [42]. This reproducible 9 minute delay for contact-activated PPP to coagulate was simulated by adding 0.03 U/mL FXIa to MP-depleted, FXII-depleted plasma, and shortened by adding 0.3 U FXIa, suggesting that the rate of FXII is a limiting factor in the reproducible maximal kinetics of coagulation in the TEG assay. Another factor in the time delay could be related to the time required for initial thrombin levels during the initiation phase, or "kindling phase", to activate cofactors FVIII and FV that are missing a gla domain [43]. After contact pathway activation of PPP, tenase, prothrombinase and prothrombin can concentrate on the surface of PS+ MPs leading to burst coagulation. Collective data indicate that HA NPs, glass beads and L-PPE:O activated the contact pathway; however this still begs the question, where did tenase, prothrombinase, and prothrombin bind in MP-depleted plasma induced to coagulate by glass beads, HA NPs and L-PPE:O containing [COO^-]?

Burst coagulation through the intrinsic pathway depends on a battery of coagulation factors that form multi-subunit assemblies, and PS plays an essential role. Among the major phospholipids phosphatidyl choline, phosphatidyl ethanolamine, and PS, PS is the only anionic lipid that can effectively mediate coagulation factor assembly although lysophosphatidyl serine can also complex with gla domain pro-coagulant factors [44]. PS is the only lipid to carry a negatively

charged carboxyl group at neutral pH (pKa 3.6) [45]. It is believed that a single PS molecule complexes with the gla domain of prothromin through the PS carboxylate group and two calcium bridging ions embedded in the gla domain while phosphates of PS and surrounding lipids serve to stabilize and orient the rest of the gla domain so that the active site presents at the optimal distance from the lipid membrane surface [44]. The PS carboxylate group therefore mediates gla domain tethering.

Gla domains carry a cluster of glutamic acid residues bearing extra carboxyl groups through a Vitamin K-dependent post-translational modification. The highly charged gla domain is folded in a tight complex with multiple calcium ions to form a binding site that latches the factor in an optimal orientation onto lipid membrane surfaces rich in anionic PS [19, 44]. Active thrombin is generated by two thrombinase cleavages, one that cleaves inside the thrombin enzyme and another that splits thrombin from the F1.2 gla domain-containing fragment [46]. According to the current modified "waterfall" model of coagulation factor activation, low levels of thrombin generated during the initiation phase feed-back activate co-factors lacking a gla domain: FXI, FV and FVIII [47-49], although the ability of thrombin to activate FXI in plasma is under debate [50]. Activation of FVa is a crucial step because FXa prothrombinase activity is exponentially ramped up by recruitment of FVa which can also complex with the gla domain of prothrombin [48, 51]. This sequence of events leads to explosive thrombin generation in the propagation phase, all provided that binding sites such as PS are available to concentrate the gla domain factors in the same physical space [52].

The active site of FVIIa bound to TF is estimated to occur at 52 to 76 Å from the plasma membrane surface. Ohkubo [19] estimated that insertion of the gla domain into the anionic lipid membrane is required for optimal alignment of the catalytic domains of coagulation factors. Both Ohkubo [19] and Baylon [56] estimated from theoretical models that coagulation factors bearing

gla domains become optimally aligned when the ω loop of the gla domain inserts into anionic membranes to a depth of around 5 to 10 Å. In this model, the calcium ions complexed with gla residues are close to the phosphate groups of lysophosphatides [19]. The ω loop may have some capacity to interact with carboxylic acid groups in L-PPE:O. The ω loop has no capacity to penetrate the smooth glass or HA NP surfaces, although is relevant to note that calcium ions can complex with PO_4^{3-} and mediate the binding of a variety of gla-domain proteins with bone mineral phosphates including SPARC (osteonectin), matrix gla protein (MGP), and gla-rich protein (GRP) [54, 55]. It is therefore possible that gla domain coagulation factors could concentrate on the surfaces of HA NPs through mechanisms that remain to be elucidated. However, given that XIa alone could stimulate burst coagulation of MP-depleted plasma in the absence of exogenous anionic surfaces, it is most probable that residual MPs remained in our MP-depleted plasma and provided sufficient phosphatidyl serine groups and/or their tissue factor to mediate gla domain factor assembly. Future experiments are warranted to clarify these physical interactions and potential role of TF.

Our study provides a new type of advanced prothrombin time (APTT) test, where in the TEG assay the kinetics of spontaneous clot initiation by trace MPs in PPP could be out-competed by 0.2 mg/mL glass microbeads to initiate a very precise clot initiation time in the TEG assay. The glass microbead TEG assay could therefore be used with PPP or MP-depleted plasma to compare the relative effect of biomaterials, activators and inhibitors on the intrinsic coagulation cascade. Future tests will show whether the glass microbead TEG assay will give similar results with clinical samples from subjects with different inflammatory states, distinct anticoagulant therapies (Coumadin, heparin, aspirin), and MP populations.

Findings in this study have some clinical relevance. The pro-coagulant activity of calcium phosphate crystals *in vivo* could serve a beneficial function of ensuring that thrombin is generated at a fractured bone mineral surface, with ensuing fibrin formation connecting the fracture with the hematoma. Shiu et al [57] have argued that fibrin clot formation plays a key role in contact osteogenesis, by serving a scaffold for continuous recruitment of osteogenic cells for direct bone deposition on an implant surface. With this notion, and the data presented here, we propose that some anionic particle-containing biomaterials could be osteogenic *in vivo* by virtue of their initial pro-thrombogenic activity at the time of implantation. Pro-coagulant activity of anionic particles wear debris could also have implications in certain painful disease states such as heterotopic ossification which occurs through unexplained mechanisms in soft tissues around healing polytraumatic bone fractures, and in osteoarthritis [58]. These data provide a new understanding of biomaterial-blood interactions and the potential impact on human health. The implication is that bone void fillers with anionic surfaces could activate the coagulation cascade to promote fibrin fibers to connect with the material and provide a scaffold for inward cell migration, because HA NPs, bioactive glass, and MPs are sufficient to mediate coagulation in the absence of platelet activation.

Role of the funding source and Acknowledgements

This work was supported by the Natural Sciences and Engineering Research Council of Canada (NSERC Discovery grant number 262874-2009 to C.D.H.), by the Canadian Institutes for Health Research (CIHR Operating grant number MOP-133729 to C.D.H.) and George Mason University Start-up funds (to C.D.H). Partial salary support for C.D.H. was from the Fonds de la Recherche Québec Santé (National Research Scientist award, grant number 22341). A.C.-G. gratefully acknowledges financial support from CONACyT (México) and from the MEDITIS Program

(NSERC and École Polytechnique) for his post-doctoral fellowship. N.L.D and P.V.M acknowledge financial support from CONICET (Argentina) and ELAP (Canada) scholarships. We thank Monica Iliescu for her valuable technical contributions for the ESEM imaging data.

Disclosures
The authors have no competing interests to declare for this paper.

Contributors
TEG data and interpretation (ACG, ND, MD, CHLF, GER, CDH)
HA NP synthesis and characterization (ND, PM)
PECVD coatings and XPS data collection (ACG, MW**)**
XPS data interpolation and interpretation (JCG, ACG, MW)
Manuscript drafting (ACG, CDH), revision (CDH, MW, ACG, ND, GER), response to reviews (CDH, GER, MW, ACG).
Approval of the final manuscript: All authors

References

[1] T.A. Ostomel, Q.H. Shi, C.K. Tsung, H.J. Liang, G.D. Stucky, Spherical bioactive glass with enhanced rates of hydroxyapatite deposition and hemostatic activity, Small 2(11) (2006) 1261-1265.
[2] C. Marchand, G.E. Rivard, J. Sun, C.D. Hoemann, Solidification mechanisms of chitosan-glycerol phosphate/blood implant for articular cartilage repair, Osteoarthritis Cartilage 17(7) (2009) 953-960.
[3] H. Peng, P. Shek, Development of in situ-forming hydrogels for hemorrhage control, Journal of Materials Science: Materials in Medicine 20(8) (2009) 1753-1762.
[4] R.J. Berckmans, A. Sturk, L.M. van Tienen, M.C.L. Schaap, R. Nieuwland, Cell-derived vesicles exposing coagulant tissue factor in saliva, Blood 117(11) (2011) 3172-3180.
[5] A. Contreras-García, Y. Merhi, J.-C. Ruiz, M.R. Wertheimer, C.D. Hoemann, Thromboelastography (TEG) Cups and Pins with Different PECVD Coatings: Effect on the Coagulation Cascade in Platelet-poor Blood Plasma, Plasma Processes and Polymers 10(9) (2013) 817-828.
[6] M.A. McMichael, S.A. Smith, Viscoelastic coagulation testing: technology, applications, and limitations, Veterinary Clinical Pathology 40(2) (2011) 140-153.
[7] G.E. Rivard, K.E. Brummel-Ziedins, K.G. Mann, L. Fan, A. Hofer, E. Cohen, Evaluation of the profile of thrombin generation during the process of whole blood clotting as assessed by thrombelastography, Journal of Thrombosis and Haemostasis 3(9) (2005) 2039-2043.
[8] A.P. Owens, N. Mackman, Microparticles in Hemostasis and Thrombosis, Circulation Research 108(10) (2011) 1284-1297.
[9] E. van der Pol, A.N. Boing, P. Harrison, A. Sturk, R. Nieuwland, Classification, Functions, and Clinical Relevance of Extracellular Vesicles, Pharmacological Reviews 64(3) (2012) 676-705.
[10] M. Yanez-Mo, P.R.M. Siljander, Z. Andreu, A.B. Zavec, F.E. Borras, E.I. Buzas, K. Buzas, E. Casal, F. Cappello, J. Carvalho, E. Colas, A. Cordeiro-da Silva, S. Fais, J.M. Falcon-Perez, I.M. Ghobrial, B. Giebel, M. Gimona, M. Graner, I. Gursel, M. Gursel, N.H.H. Heegaard, A. Hendrix, P. Kierulf, K. Kokubun, M. Kosanovic, V. Kralj-Iglic, E.M. Kramer-Albers, S. Laitinen, C. Lasser, T. Lener, E. Ligeti, A. Line, G. Lipps, A. Llorente, J. Lotvall, M. Mancek-Keber, A. Marcilla, M. Mittelbrunn, I. Nazarenko, E.N.M. Nolte-t' Hoen, T.A. Nyman, L. O'Driscoll, M. Olivan, C. Oliveira, E. Pallinger, H.A. del Portillo, J. Reventos, M. Rigau, E. Rohde, M. Sammar, F. Sanchez-Madrid, N. Santarem, K. Schallmoser, M.S. Ostenfeld, W. Stoorvogel, R. Stukelj, S.G. Van der Grein, M.H. Vasconcelos, M.H.M. Wauben, O. De Wever, Biological properties of extracellular vesicles and their physiological functions, Journal of Extracellular Vesicles 4 (2015).
[11] E. Chargaff, R. West, The Biological Significance of the Thromboplastic Protein of Blood, Journal of Biological Chemistry 166 (1946) 189-197.
[12] R. Nieuwland, R.J. Berckmans, R.C. RotteveelEijkman, K.N. Maquelin, K.J. Roozendaal, P.G.M. Jansen, K. tenHave, L. Eijsman, C.E. Hack, A. Sturk, Cell-derived microparticles generated in patients during cardiopulmonary bypass are highly procoagulant, Circulation 96(10) (1997) 3534-3541.
[13] R. Nieuwland, R.J. Berckmans, S. McGregor, A.N. Boing, F. Romijn, R.G.J. Westendorp, C.E. Hack, A. Sturk, Cellular origin and procoagulant properties of microparticles in meningococcal sepsis, Blood 95(3) (2000) 930-935.
[14] S. Nomura, M. Shimizu, Clinical significance of procoagulant microparticles, J. Intensive Care 3 (2015) 11.
[15] Y. Zhang, H. Meng, R. Ma, Z. He, X. Wu, M. Cao, Z. Yao, L. Zhao, T. Li, R. Deng, Z. Dong, Y. Tian, Y. Bi, J. Kou, H.S. Thatte, J. Zhou, J. Shi, Circulating Microparticles, Blood Cells, and Endothelium Induce Procoagulant Activity in Sepsis Through Phosphatidylserine Exposure, Shock 45(3) (2016) 299-307.
[16] T. Nielsen, A.F. Kristensen, S. Pedersen, G. Christiansen, S.R. Kristensen, Investigation of procoagulant activity in extracellular vesicles isolated by differential ultracentrifugation, Journal of Extracellular Vesicles 7(1) (2018).

[17] M.J. Mooberry, N.S. Key, Microparticle Analysis in Disorders of Hemostasis and Thrombosis, Cytometry Part A 89A(2) (2016) 111-122.
[18] N. Tavoosi, R.L. Davis-Harrison, T.V. Pogorelov, Y.Z. Ohkubo, M.J. Arcario, M.C. Clay, C.M. Rienstra, E. Tajkhorshid, J.H. Morrissey, Molecular Determinants of Phospholipid Synergy in Blood Clotting, Journal of Biological Chemistry 286(26) (2011) 23247-23253.
[19] Y.Z. Ohkubo, E. Tajkhorshid, Distinct structural and adhesive roles of Ca2+ in membrane binding of blood coagulation factors, Structure 16(1) (2008) 72-81.
[20] A.C.W. Pike, A.M. Brzozowski, S.M. Roberts, O.H. Olsen, E. Persson, Structure of human factor VIIa and its implications for the triggering of blood coagulation, Proc. Natl. Acad. Sci. U. S. A. 96(16) (1999) 8925-8930.
[21] R.W. Colman, A.W. Clowes, J.N. George, J. Hirsh, V.J. Marder, Overview of Hemostasis, in: R.W. Colman, J. Hirsh, V.J. Marcer, A.W. Clowes, J.N. George (Eds.), Hemostasis and Thrombosis; Basic Principles and Clinical Practice, Lippincott Williams & Wilkins, New York, 2001, pp. 3-16.
[22] N.L. D'Elia, A.N. Gravina, J.M. Ruso, J.A. Laiuppa, G.E. Santillan, P.V. Messina, Manipulating the bioactivity of hydroxyapatite nano-rods structured networks: Effects on mineral coating morphology and growth kinetic, Biochimica Et Biophysica Acta-General Subjects 1830(11) (2013) 5014-5026.
[23] S.H. Behrens, D.G. Grier, The charge of glass and silica surfaces, Journal of Chemical Physics 115(14) (2001) 6716-6721.
[24] E.A. Vogler, C.A. Siedlecki, Contact activation of blood-plasma coagulation, Biomaterials 30(10) (2009) 1857-1869.
[25] D.H. Ryan, Examination of the Blood, in: E. Bueter, B.S. Coller, M.A. Lichtman, T.J. Kipps, U. Seligsohn (Eds.), Williams, Hematology, McGraw-Hill Medical Publishing Division2001.
[26] C. Maas, T. Renne, Coagulation factor XII in thrombosis and inflammation, Blood 131(17) (2018) 1903-1909.
[27] Y.Z. Wang, L.T. Luo, O.O. Braun, J. Westman, R. Madhi, H. Herwald, M. Morgelin, H. Thorlacius, Neutrophil extracellular trap-microparticle complexes enhance thrombin generation via the intrinsic pathway of coagulation in mice, Scientific Reports 8 (2018).
[28] O.D. Ratnoff, J.M. Rosenblum, Role of Hageman Factor in the Initiation of Clotting by Glass: Evidence that glass frees hageman factor from inhibition, Am. J. Medicine 25 (1958) 160-168.
[29] C.-H.J. Yeh, Z.O. Dimachkie, A. Golas, A. Cheng, P. Parhi, E.A. Vogler, Contact Activation of Blood Plasma and Factor XII by Ion-exchange Resins, Biomaterials 33(1) (2012) 9-19.
[30] M.A. Panteleev, M.V. Ovanesov, D.A. Kireev, A.M. Shibeko, E.I. Sinauridze, N.M. Ananyeva, A.A. Butylin, E.L. Saenko, F.I. Ataullakhanov, Spatial propagation and localization of blood coagulation are regulated by intrinsic and protein C pathways, respectively, Biophys J 90(5) (2006) 1489-500.
[31] F. Muller, N.J. Mutch, W.A. Schenk, S.A. Smith, L. Esterl, H.M. Spronk, S. Schmidbauer, W.A. Gahl, J.H. Morrissey, T. Renne, Platelet Polyphosphates Are Proinflammatory and Procoagulant Mediators In Vivo, Cell 139(6) (2009) 1143-1156.
[32] C. Oslakovic, T. Cedervall, S. Linse, B. Dahlback, Polystyrene nanoparticles affecting blood coagulation, Nanomedicine-Nanotechnology Biology and Medicine 8(6) (2012) 981-986.
[33] R. Ito, B.E. Statland, Centrifugal analysis for plasma kallikrein activity, with use of the chromogenic substrate S-2301, Clinical Chemistry 27(4) (1981) 586-593.
[34] A. Yang, J. Dai, Z. Xie, R.W. Colman, Q. Wu, R.B. Birge, Y. Wu, High molecular weight kininogen binds phosphatidylserine and opsonizes urokinase plasminogen activator receptor-mediated efferocytosis, Journal of immunology (Baltimore, Md. : 1950) 192(9) (2014) 4398-408.
[35] K.A. Mitropoulos, M.P. Esnouf, THE AUTOACTIVATION OF FACTOR-XII IN THE PRESENCE OF LONG-CHAIN SATURATED FATTY-ACIDS - A COMPARISON WITH THE POTENCY OF SULFATIDES AND DEXTRAN SULFATE, Thrombosis and Haemostasis 66(4) (1991) 446-452.

[36] R.E. Thompson, R.J. Mandle, A.P. Kaplan, Association of Factor XI and High Molecular Weight Kininogen in Human Plasma, Journal of Clinical Investigation 60 (1977) 1376-1380.
[37] C.F. Scott, L.D. Silver, M. Schapira, R.W. Colman, Cleavage of human high molecular weight kininogen markedly enhances its coagulant activity. Evidence that this molecule exists as a procofactor, J Clin Invest 73(4) (1984) 954-62.
[38] K.A. Mitropoulos, The levels of factor XIIa generated in human plasma on an electronegative surface are insensitive to wide variation in the concentration of FXII, prekallikrein, high molecular weight kininogen or FXI, Thromb Haemost 82(3) (1999) 1033-40.
[39] C.F. Scott, L.D. Silver, A.D. Purdon, R.W. Colman, Cleavage of human high molecular weight kininogen by factor XIa in vitro. Effect on structure and function, The Journal of biological chemistry 260(19) (1985) 10856-63.
[40] J.H. Griffin, Role of surface in surface-dependent activation of Hageman factor (blood coagulation factor XII), Proc Natl Acad Sci U S A 75(4) (1978) 1998-2002.
[41] B. Osterud, B.N. Bouma, J.H. Griffin, Human blood coagulation factor IX. Purification, properties, and mechanism of activation by activated factor XI, The Journal of biological chemistry 253(17) (1978) 5946-51.
[42] D.J. Fletcher, K.J. Blackstock, K. Epstein, B.M. Brainard, Evaluation of tranexamic acid and epsilon-aminocaproic acid concentrations required to inhibit fibrinolysis in plasma of dogs and humans, American Journal of Veterinary Research 75(8) (2014) 731-738.
[43] K.G. Mann, K. Brummel, S. Butenas, What is all that thrombin for?, Journal of Thrombosis and Haemostasis 1(7) (2003) 1504-1514.
[44] M.D. Huang, A.C. Rigby, X. Morelli, M.A. Grant, G.Q. Huang, B. Furie, B. Seaton, B.C. Furie, Structural basis of membrane binding by Gla domains of vitamin K-dependent proteins, Nature Structural Biology 10(9) (2003) 751-756.
[45] F.C. Tsui, D.M. Ojctus, W.L. Hubbel, The Intrinsic pKa Values for Phosphatidylserine and Phosphatidylethanolamine in Phosphatidylcholine Host Bilayers, Biophysical Journal 49 (1986) 459-468.
[46] L.M. Haynes, B.A. Bouchard, P.B. Tracy, K.G. Mann, Prothrombin Activation by Platelet-associated Prothrombinase Proceeds through the Prethrombin-2 Pathway via a Concerted Mechanism, Journal of Biological Chemistry 287(46) (2012) 38647-38655.
[47] D.E. Davies, O.D. Ratnoff, Waterfall Sequence for Intrinsic Blood Clotting, Science 145(3638) (1964) 1310-1312.
[48] S. Butenas, C. vantVeer, K.G. Mann, Evaluation of the initiation phase of blood coagulation using ultrasensitive assays for serine proteases, Journal of Biological Chemistry 272(34) (1997) 21527-21533.
[49] J.H. Morrissey, S.H. Choi, S.A. Smith, Polyphosphate: an ancient molecule that links platelets, coagulation, and inflammation, Blood 119(25) (2012) 5972-5979.
[50] D.L. Pedicord, D. Seiffert, Y. Blat, Feedback activation of factor XI by thrombin does not occur in plasma, Proc. Natl. Acad. Sci. U. S. A. 104(31) (2007) 12855-12860.
[51] M.D. Blostein, A.C. Rigby, M. Jacobs, B. Furie, B.C. Furie, The Gla domain of human prothrombin has a binding site for factor Va, Journal of Biological Chemistry 275(48) (2000) 38120-38126.
[52] F. London, S.S. Ahmad, P.N. Walsh, Annexin V inhibition of factor IXa-catalyzed factor X activation on human platelets and on negatively-charged phospholipid vesicles, Biochemistry 35(51) (1996) 16886-16897.
[53] M. Shiozawa, H. Takahashi, N. Iwasaki, T. Wada, M. Uo, Effect of immersion time of restorative glass ionomer cements and immersion duration in calcium chloride solution on surface hardness, Dental Materials 30(12) (2014) E377-E383.
[54] D.D. Stenner, R.P. Tracy, B.L. Riggs, K.G. Mann, Human platelets contain and secrete osteonectin, a major protein of mineralized bone, Proceedings of the National Academy of Sciences 83(18) (1986) 6892-6896.

[55] S. Cavaco, C.S.B. Viegas, M.S. Rafael, A. Ramos, J. Magalhes, F.J. Blanco, C. Vermeer, D.C. Simes, Gla-rich protein is involved in the cross-talk between calcification and inflammation in osteoarthritis, Cellular and Molecular Life Sciences 73(5) (2016) 1051-1065.
[56] J.L. Baylon, J.V. Vermaas, M.P. Muller, M.J. Arcario, T.V. Pogorelov, E. Tajkhorshid, Atomic-level description of protein-lipid interactions using an accelerated membrane model, Biochimica Et Biophysica Acta-Biomembranes 1858(7) (2016) 1573-1583.
[57] H.T. Shiu, B. Goss, C. Lutton, R. Crawford, Y. Xiao, Formation of Blood Clot on Biomaterial Implants Influences Bone Healing, Tissue Engineering Part B-Reviews 20(6) (2014) 697-712.
[58] S. Agarwal, M. Sorkin, B. Levi, Heterotopic Ossification and Hypertrophic Scars, Clin. Plast. Surg. 44(4) (2017) 749-+.

Figure Legends

Figure 1: Kinetics of fibrin fiber formation influence different stages of the TEG trace. Panel (A) shows stages of coagulation and fibrin fiber formation in the TEG assay in a representative trace of recalcified citrated platelet-poor blood plasma sample. Panel (B) depicts the sequential process of fibrin polymerization after thrombin-induced cleavage of telopeptides A and B from the fibrinogen hexamer precursor. Pro-coagulant activity can be demonstrated by a shorter clotting time (R), shorter time to attain 20 mm amplitude (K), and high alpha (α, angle, red lines).

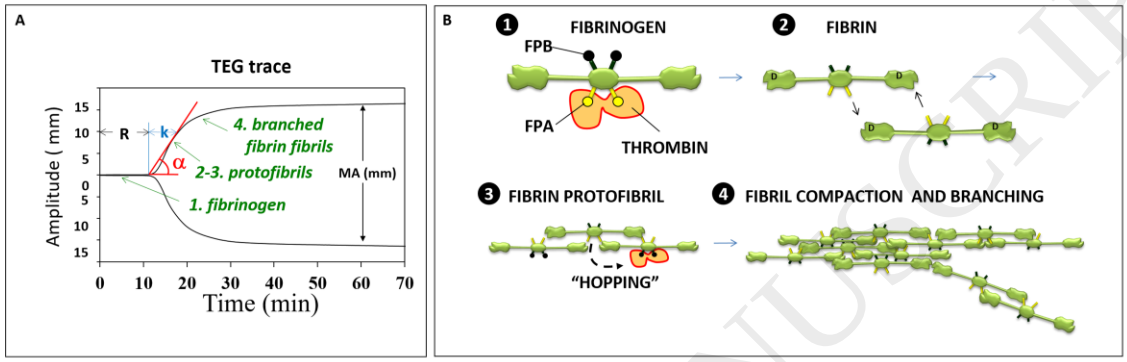

Figure 2. Ultrastructure of the pelleted formalin-fixed MP fraction by ESEM imaging (A) and representative TEG traces of recalcified citrated PPP, MP-enriched, and MP-depleted plasma permitted to coagulate spontaneously in the Cyrolite plastic TEG cup and pin (B). PPP and MP-enriched plasma coagulated spontaneously but MP-depleted plasma failed to coagulate.

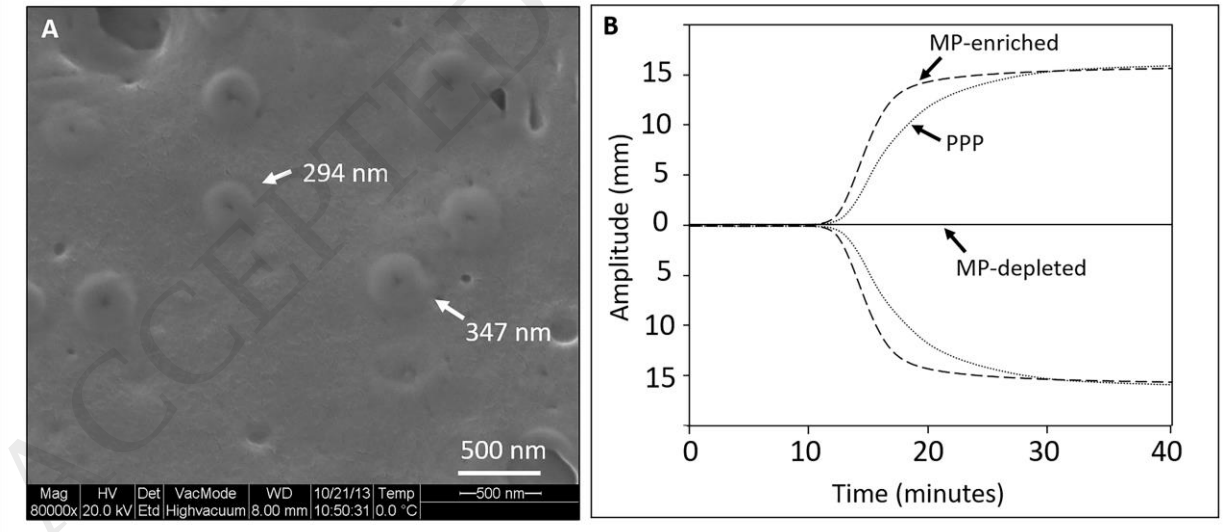

Figure 3. High resolution X-ray photon spectroscopy (C1s and O1s) spectra for L-PPE:O coatings: a) *R*= 0.025, b) *R*= 0.050,and c) *R*= 0.075. Peak E representing the carboxylic acid group is only detected for b) *R*= 0.050,and c) *R*= 0.075.

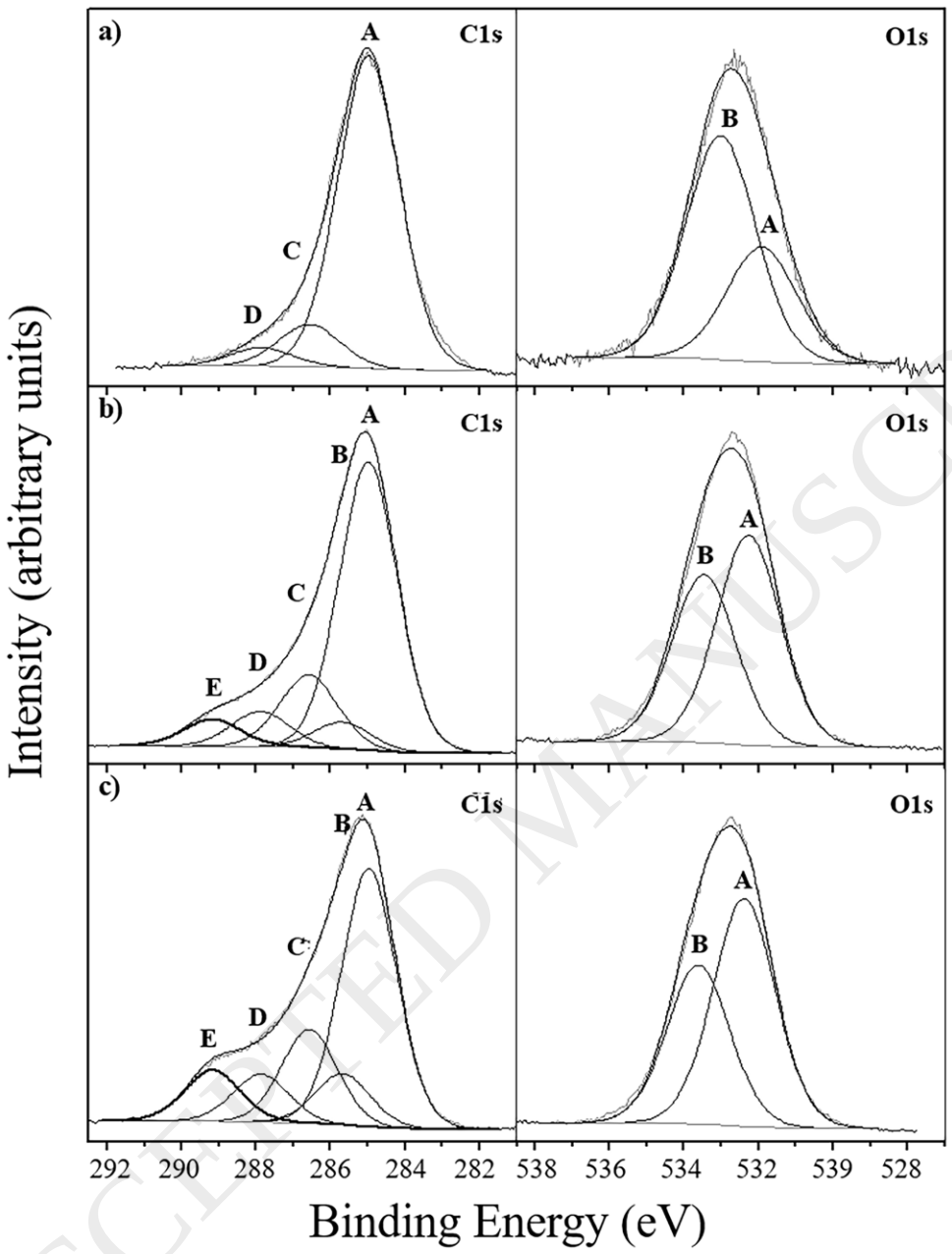

Figure 4. TEG assay of PPP coagulation in the presence of different surfaces. Coagulation was accelerated by synthetic anionic surfaces and delayed by hydrophobic surfaces, relative to the conventional Cyrolite TEG cup and pin surfaces. (A) HA NPs accelerated PPP coagulation in a dose-dependent manner. These data are the first to our knowledge to show that hydroxyapatite is a pro-coagulant surface that accelerates PPP coagulation. N=4 each condition except 25 mg/mL was N=5. (B) Anionic surfaces provided by glass beads and L-PPE:O (*R*= 0.075, 6.8 atomic % [COO^-]) stimulated PPP coagulation while hydrophobic (CYR, H, LB) and hydrophilic uncharged surfaces (CB) slightly delayed coagulation. *Abbreviations:* MA: maximal amplitude;

R: clotting time; α (alpha): angle of burst coagulation; CYR: Cyrolite® TEG cups and pins; H: PP-HMDSO-coated TEG cups and pins; LB: latex beads; CB*: CML carboxylated latex beads that only carry a net negative charge at alkaline pH (pH 10); GB: Glass microbeads; PPEO: *R*= 0.075 L-PPE:O-coated TEG cups and pins. Sample characteristics: See Table 1.

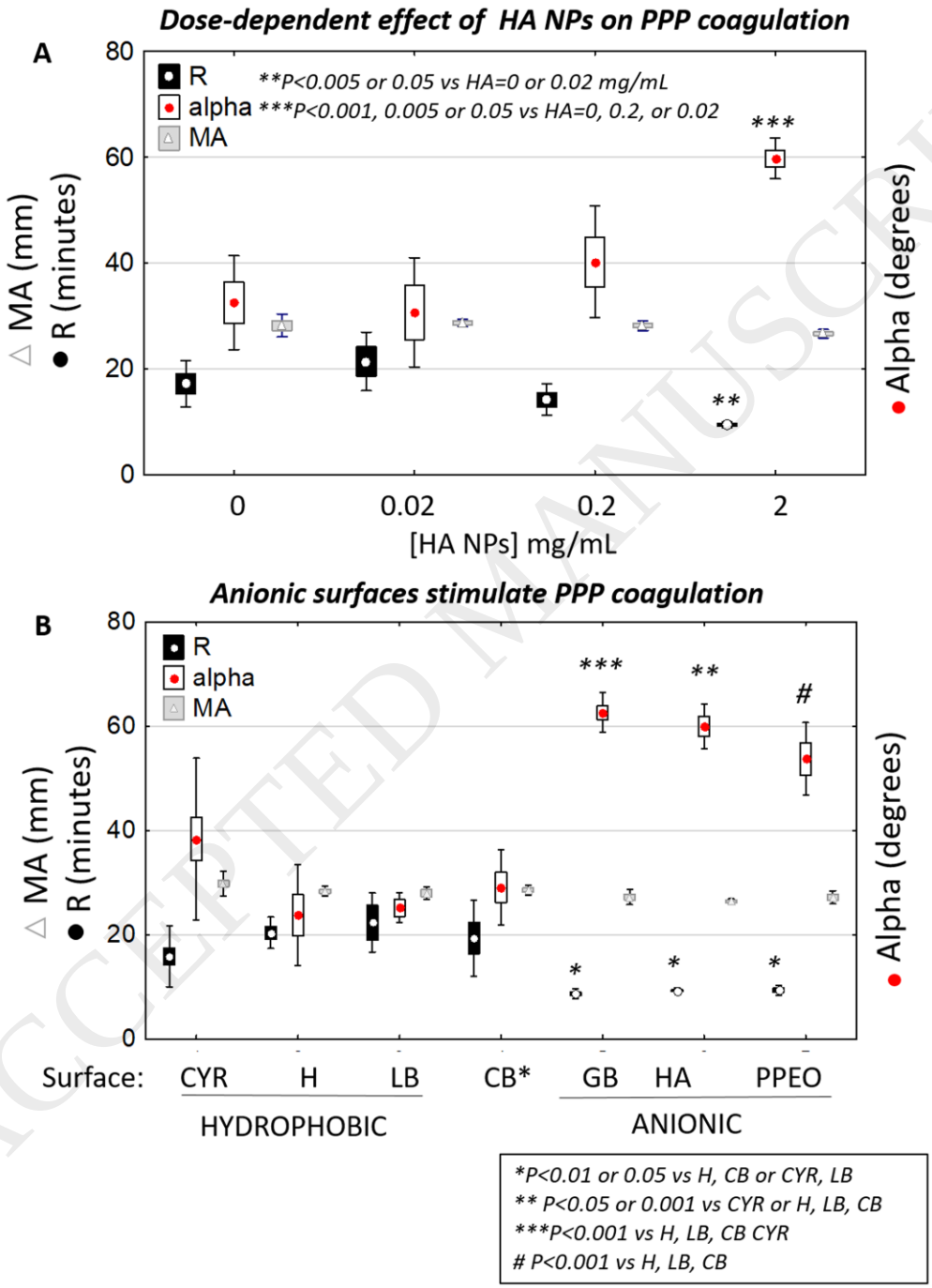

Figure 5. TEG assay of MP-depleted plasma coagulation in the presence of different surfaces. Anionic surfaces accelerated coagulation of MP-depleted plasma while hydrophilic surfaces lacking free carboxyl groups and hydrophobic surfaces failed to induce coagulation in the

Cyrolite TEG cup. (A) All L-PPE:O nanocoatings have oxygen content but only those with [COO^-] content, and HA NPs at the highest concentration, restored burst coagulation of MP-depleted plasma. (B) Glass microbeads, HA NPs and L-PPE:O (R=0.075), but not non-anionic surfaces, induced MP-depleted plasma coagulation that was comparable to PPP and MP-enriched PPP. *Abbreviations:* MA: maximal amplitude; R: clotting time; α (alpha): degrees of inflection of the TEG curve where higher angles reflect higher clot velocity; CYR: Cyrolite® TEG cups and pins; LB: latex beads; H: HMDSO-coated TEG cups and pins; CB*: carboxylic acid modified latex beads are uncharged at neutral pH; GB: glass microbeads HA: hydroxyapatite nanoparticles; PPEO: L-PPE:O-coated TEG cups and pins; MP: Microparticles; PPP: platelet-poor plasma; E-PPP: MP-enriched plasma.

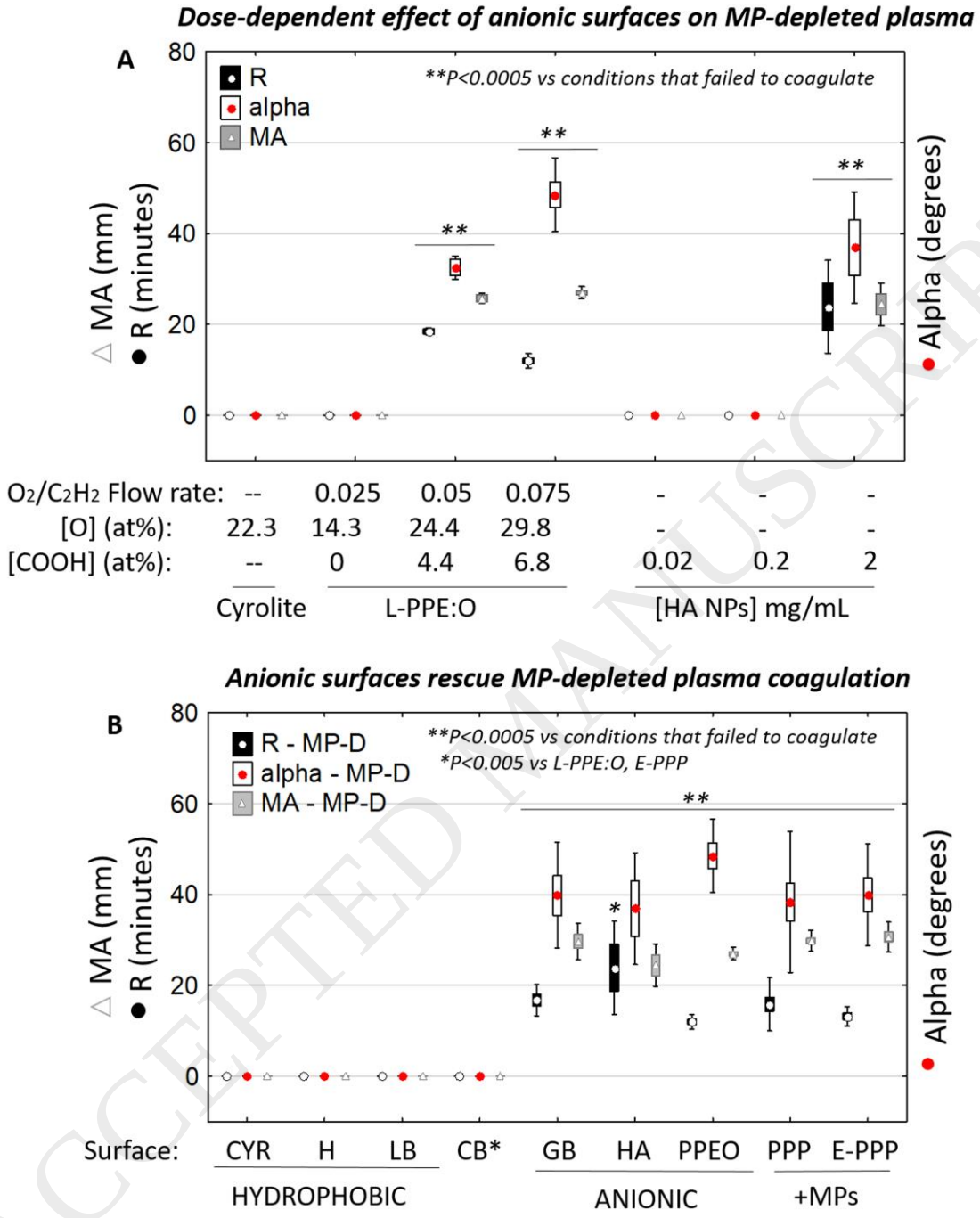

Figure 6. TEG traces of burst coagulation of MP-depleted plasma including (A) MP-depleted plasma and (B) FXII-depleted plasma(A) All 3 types of anionic surface induced explosive thrombin generation in MP-depleted plasma including L-PPE:O at increasing [COO^{-}] (in at%), glass microbeads, and HA NPs. (B) FXIa was necessary and sufficient to induce burst coagulation in a dose-dependent manner of FXII-depleted, MP-depleted plasma with no effect of added glass microbeads.

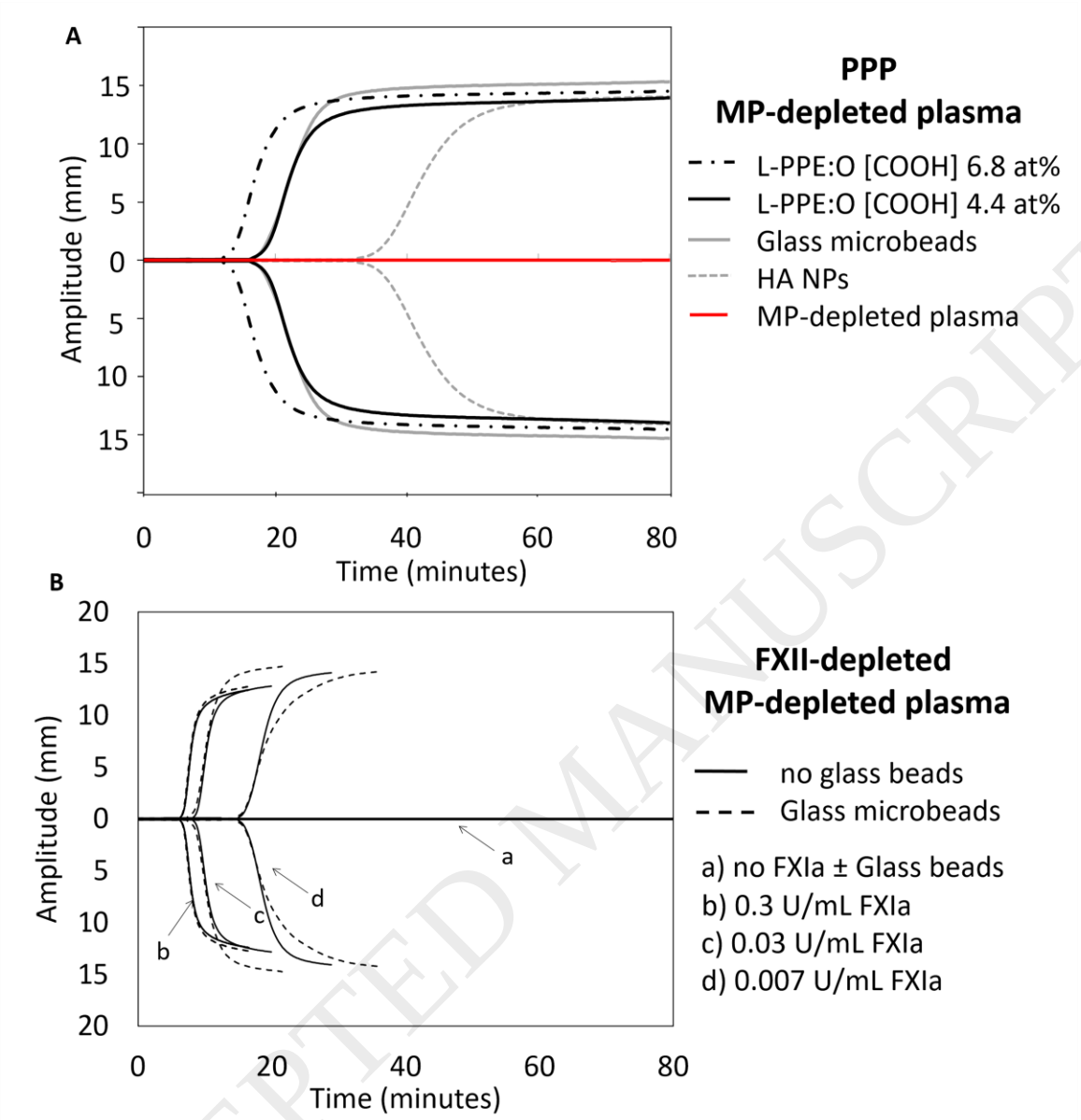

Figure 7. ESEM high-magnification imaging of PPP clots (A-C) and MP-depleted plasma clots (D-F) formed in the presence of glass microbeads showed a similar fibrin clot structure. Both thick and thin branched fibrin strands adhered to the glass beads. Small arrows in Panels A & C indicate glass beads; arrow in panel C indicates aggregated spherical structures near the top of the sample that could be lipids.

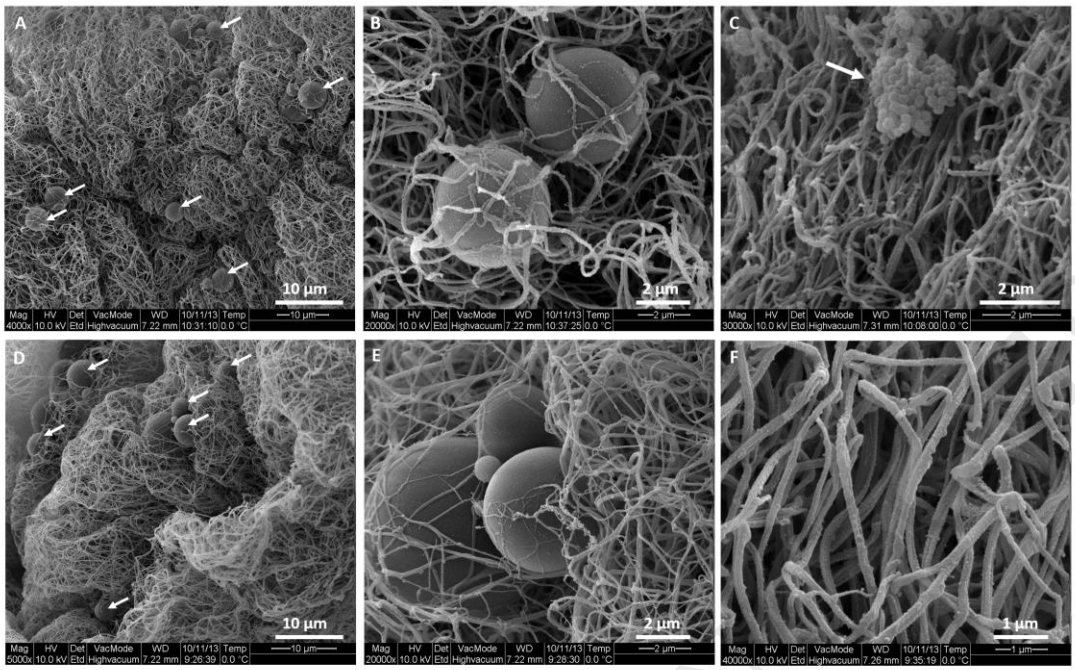

Table

Table 1. Materials tested for pro-coagulant activity in PPP or MP-depleted plasma.

Surface tested	Supplier	Character	Surface type
Cyrolite®	Haemscope	hydrophobic	bare TEG cup and pin
PP-HMDSO	In-house	hydrophobic	TEG cup and pin surface nanocoating; glass bead coating
L-PPE:O	In-house	hydrophilic/anionic 0, 4.4, or 6.8 at% [COO^-]	TEG cup and pin surface nanocoating
Latex (polystyrene) beads	Sigma-Aldrich	hydrophobic	10 µm diameter beads
Carboxylated CML latex beads*	Life Sciences	hydrophobic/hydrophilic	10 µm diameter beads
Glass microbeads	Matweb	hydrophilic/anionic	10 µm diameter beads
HA nanoparticles (MIV CTAB/IGEPAL-based crystals)	In-house	hydrophilic/anionic (2.03 Ca/P)	41 nm length, 9 nm diameter nano-cylinders

* According to the COA: 6.8 x 10^8 COOH/bead with a hydrophilic surface at neutral pH but COOH is fully charged only at pH 10; according to our XPS measures, CML beads had <1 at% COOH. at%: atomic %. Ca/P: calcium phosphate

Table 2. Parameters used to deposit L-PPE:O and PP-HMDSO on TEG cups and pins by PECVD, and corresponding Water Contact Angle (WCA) values.

Surface / Deposit	Gas flows (sccm)	r. f. power (W)	Pressure (mTorr)	Deposition time (min)	WCA (°)
Cyrolite®	--	--	--	--	77±1
L-PPE:O *R*=0.025	Ethylene - 20 Oxygen - 0.5*	10	600	20	64±1
L-PPE:O *R*=0.050	Ethylene - 20 Oxygen - 1.0*	10	600	40	51±2
L-PPE:O *R*=0.075	Ethylene - 20 Oxygen - 1.5*	10	600	60	45±1
PP-HMDSO	HMDSO - 20	50	60	2	98±2

Abbreviations: sccm: standard cubic centimeters per minute; *produced by a mixture of 10% O_2 and 90% Ar, and variable O_2/Ar gas flow

Table 3. Elemental composition of Cyrolite® and L-PPE:O deposits with different oxygen flow rates (R=O_2/C_2H_4): R= 0.025, R= 0.050, and R= 0.075.

Element	C1s (at.%)	O1s (at.%)
Cyrolite	77.7±2.5	22.3±2.5
R = 0.025	85.7±0.9	14.3±0.9
R = 0.050	76.9±1.9	24.4±0.8
R = 0.075	70.2±0.8	29.8±0.8

Table 4. C1s- and O1s-deconvolutions of L-PPE:O deposits for R= 0.025, R= 0.050, and R= 0.075, component concentrations, possible chemical bonds and binding energies (BE)

Element	C1s					O1s	
Peak label	A	B	C	D	E	A	B
Peak BE (eV)	285.0	285.7	286.6	287.9	289.2	531.9-532.4	533.0-533.6
Possible chemical bond	C-C	C-COOR	C-OR	C=O	COOR	O=C	O-C
R= 0.025 (at.%)	71.0±1.3	-----	9.8±0.1	4.5±0.4	------	5.2±0.6	9.6±0.3
R= 0.05 (at.%)	50.6±2.0	4.4±0.2	11.7±1.1	6.2±0.3	4.4±0.2	14.0±0.6	10.7±0.2
R= 0.075 (at.%)	36.5±0.9	6.8±0.4	12.7±0.5	6.8±0.2	6.8±0.4	17.9±0.2	12.6±0.1
Cryolite®	47.2	9.8	10.8	-	9.8	11.3	11.0

Table 5. Elemental composition of 500 µm diameter glass beads, unmodified and after coating with PP-HMDSO

Unmodified glass beads (at. %)	PP-HMDSO coated glass beads (at. %)
[Si]=16	[SiO_2]=1.57
[O]=45	[$SiO_{1.5}C$]=5.5
[C]=37	[$SiOC_2$]=5.5
[Ca]=1	[$SiO_{0.5}C_3$]=5.5
[Na]=0.5	